Hindawi
Shock and Vibration
Volume 2018, Article ID 4894078, 7 pages
https://doi.org/10.1155/2018/4894078

Research Article

Full Field Strain Analysis of Blasting Under High Stress Condition Based on Digital Image Correlation Method

Liyun Yang,[1] Chenxi Ding,[1] Renshu Yang,[1] Zhen Lei,[2] and Jing Wang[1]

[1]*School of Mechanics and Civil Engineering, China University of Mining and Technology (Beijing), Beijing 100083, China*
[2]*Institute of Mining Engineering, Guizhou Institute of Technology, Guizhou 550003, China*

Correspondence should be addressed to Chenxi Ding; dingcx91@sina.com

Received 30 June 2018; Revised 27 August 2018; Accepted 4 September 2018; Published 3 December 2018

Academic Editor: Chengzhi Shi

Copyright © 2018 Liyun Yang et al. This is an open access article distributed under the Creative Commons Attribution License, which permits unrestricted use, distribution, and reproduction in any medium, provided the original work is properly cited.

The depth of mineral resources like coal continuously increases due to the exhaustion of shallow resources, and the characteristic of high ground stress in deep ground inevitably affects fracture of rock blasting. Combining with high-speed photography technology, the digital image correlation method (DIC) is introduced into experimental study on explosive mechanics. And strain evolution process of blasting under high stress condition is obtained by using the model experiment method. The preliminary results show that high stress condition has no obvious effects on the propagation law of blasting stress wave or its stress peak in the medium. In addition, it is found that medium in the "elastic vibration area" by conventional blast zoning is not always "elastic," and on this basis, the concepts of "plastic area" and "quasielastic area" are put forward. The high stress condition does not influence partition range of above "plastic area" or "quasielastic area," but in the "plastic area," the high stress condition decreases both plastic strain value and its decay rate of relevant gauging points.

1. Introduction

In recent years, the state of mineral resource exploitation like coal is shifted from the open air to the underground and from the shallow to the deep; resource exploitation environment is more complex, and the exploitation difficulty increases dramatically. He [1] pointed out that the high ground stress is a significant difference between deep mining and shallow mining, which is also a problem that must be faced and solved by deep mining. With deepening of resource exploitation, corresponding construction methods also need to consider the characteristics of deep mining and make technological innovation to better serve high efficient utilization of resource. Drilling and blasting, as a traditional and effective construction method, is widely used in rock crushing and rock roadway excavation. In the process of blasting excavation of an underground hydropower station, Lu [2] found that the high ground stress is one of the main reasons for crack expansion in contour blasting and considered it is unreasonable for deep rock blasting design according to shallow rock blasting parameters when the ground stress exceeds 10–12 MPa. Nevertheless, in current deep rock blasting construction, the design of blasting parameters does not take the impact of high ground stress into account, resulting in unreasonable use of explosive energy and poor blasting effect.

Many scholars and researchers have noticed that the high ground stress cannot be ignored for rock blasting [3–10]. Kutter [3] published a classical literature about the blasting failure mechanism, in which he found the crack propagation gave priority in the direction of maximum principal stress in static stress field by using polymethyl methacrylate (PMMA) and rock materials. Bai [4] also found the ground stress field has a guiding effect on the expansion of blasting induced crack, and main direction of the crack propagation tends to the direction of the maximum principal stress. It is thought that the increase of hole spacing or reduction of the charge amount in the direction of the maximum principal stress can improve blasting quality and reduce explosive consumption [5]. Yan [6] believed that the coupling effect of blasting loading and high ground stress on damage of the surrounding rock is greater than the effect of

their linear superposition. Wei [7] carried out the numerical simulation of slit-charge blasting under different high stress conditions, it is found that the crack propagation direction is controlled by the incision angle and the direction of maximum ground stress, and the crack propagation scale is mainly controlled by the value of ground stress.

From the existing research, the study of deep rock blasting response is focused on expansion of blasting induced cracks. Due to the limitations of relevant test methods and experimental equipment, influence of high stress condition on blasting stress wave propagation is rarely studied. In this paper, the full field strain evolution of blasting under high stress condition is analyzed by model experiment with experimental system of high-speed digital image correlation.

2. Experiment Introduction

2.1. Experimental System. In recent years, the digital image correlation method (DIC) [11–14] has been successfully applied to experimental research in many fields as an effective optical testing technology and has become an important test method for modern photometric mechanics. The basic measurement principle of DIC is that speckle field is made on the surface of the specimen before experiment, and then an image acquisition system is used to collect the speckle patterns before and after deformation of the object. After the image processing, the speckle patterns are transformed into two digital gray fields. Through correlation processing of the gray fields, the displacement field of object surface is obtained. Then, according to the relationship between displacement and strain, the strain field of object surface is obtained.

From existing literature records, DIC method has been gradually applied to the study of blasting problem. Based on the high-speed DIC, He [15] performed a laboratory experiment to investigate the dynamic response of rock subjected to couple static and dynamic stresses from active confining pressure and blasting. In addition, by using high-speed 3D DIC, the crack propagation process and the 3D deformation characteristics of cylindrical concrete specimens under blast loading were analyzed [16].

As shown in Figure 1, the experimental system of high-speed digital image correlation used in this experiment is mainly composed of high-speed camera, VIC-2D analysis software, lighting system, and synchronous control system.

(1) Kirana-5M high-speed camera. The camera uses μCMOS sensor, and it is possible to realize high-speed acquisition without lowering the image resolution. Its image resolution is fixed to 924 pixels × 768 pixels, the number of acquisition is 180, and the fastest shooting speed is 5×10^6 fps. The shutter time of the high-speed camera in this experiment is 1 μs.

(2) VIC-2D software. The software has the function of automatically calibrating the scale factor of the graph and uses the normalized squared correlation function to carry on the correlation calculation, which is not sensitive to bright light change. The optimal calculation is carried out under the premise of satisfying the accuracy and the calculation speed. This software is widely used in digital image correlation analysis at home and abroad.

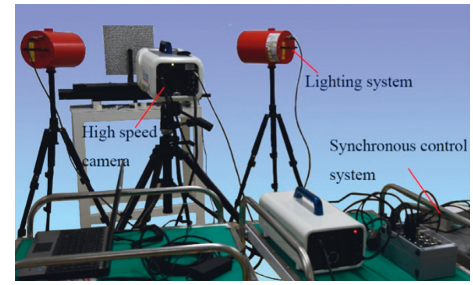

Figure 1: Experimental system of high-speed digital image correlation.

(3) SI-AD500 lighting system. The system consists of a controller and a flash. The controller is a four-channel CU-500 controller that can control multi-channel simultaneous or sequential operation. The flash is FH-500 xenon lamp, which can achieve 2 ms constant light intensity of lighting time to ensure the ultra-high-speed camera on the exposure requirements.

(4) Synchronous control system. The operation of high-speed camera poses a high demand for synchronous control. The HD 12-2 synchronous control system is designed and developed by our team, and it can set startup sequence and delay time of the explosive initiation, the camera, and the lighting system.

For blast research, a start trigger mode was used in the experimental system. When the trigger signal is manually given, the lighting system is initiated. After 50–100 μs, the intensity of the light field reaches a steady value, and the high-speed camera begins to acquire images, whereupon the explosive in the specimen blasthole is detonated.

Figure 2 presents the front view of the self-designed dynamic-static loading device, which can apply dynamic blasting stress and static compressive stress on the specimen. The dynamic blasting stress is generated by the detonation of explosive in the middle of the specimen, and the static compressive stress is provided by jack. A stress sensor with a range of 5t, and an accuracy of 0.1 kg is used for real-time measurement of the compressive stress. In addition, the jack can also record the reading of the pressure sensor and do some relevant conversions. Through calculation, the σ applied by jack which is regarded as an equivalent principal stress difference can be obtained. The lead azide ($Pb(N_3)_2$) is placed in the borehole of specimen and blocked with the jig, and then the detonation is achieved by high voltage discharge. The related parameters of $Pb(N_3)_2$ are listed in Table 1.

2.2. Specimen Parameters. The model material used in this experiment is polycarbonate (PC), and related material parameters of PC are shown in Table 2. The specimen size is

Figure 2: Dynamic-static loading system.

Table 1: Related parameters of $Pb(N_3)_2$.

Specific volume of explosion (L/kg)	Explosion heat (kJ/kg)	Explosion temperature (°C)	Explosive velocity (m/s)
308	1524	3050	4478

Table 2: Related material parameters of PC.

Density (Kg/m^3)	P-wave velocity (m/s)	S-wave velocity (m/s)	Dynamic elastic modulus (GPa)	Dynamic shear modulus (GPa)	Dynamic Poisson's ratio
1449	2125	1090	4.548	1.722	0.321

315 mm×285 mm×8 mm, and a borehole with $d = 5$ mm in diameter is prefabricated in the center.

The speckle is printed on the surface of specimen using the UV plate printing technique; the speckle diameter is 1.2 mm, the speckle density is 75%, and the speckle irregularity is 75%. The size of the subset used in the experiment is 29×29 pixels, and the calculation step is 7 pixels. Two groups of specimens are designed in the experiment, specimen T1 ($\sigma = 0$ MPa, under normal stress condition) and specimen T2 ($\sigma = 6$ MPa, under high stress condition). Eight gauging points are selected in each specimen for strain monitoring as shown in Figure 3. The polar coordinate system is established with the center of borehole as the coordinate origin. The distance s between gauging points G1, G2, G3,···, G8 and the borehole is respectively 35 mm (7d), 40 mm (8d), 45 mm (9d), and 70 mm (14d).

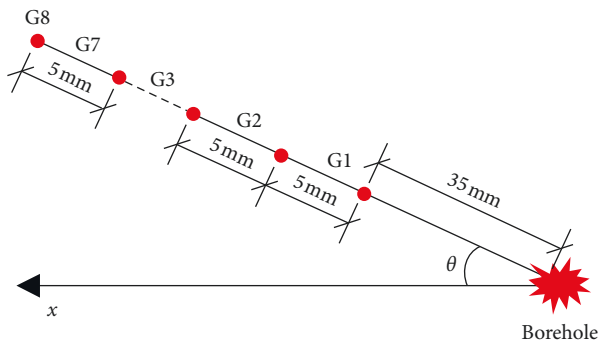

Figure 3: Diagram of gauging point position.

3. Experiment Analysis

3.1. Strain Evolution. The explosive initiation time is $t = 0$ μs, and Figure 4 shows the maximum principal strain under the action of blasting stress wave at different time. The measurement accuracy of full field strain by DIC method depends on the image resolution and speckle quality. The image resolution of the experiment system is 924 pixels × 768 pixels, and the pixel size is 30 μm × 30 μm. Before the blasting experiment, speckle quality needs to be calibrated. Figure 5 is the calibrated strain curve, which shows that the measurement error of the radial strain does not exceed ±20 με and the measurement error of the circumferential strain does not exceed ±10 με. It proves that the

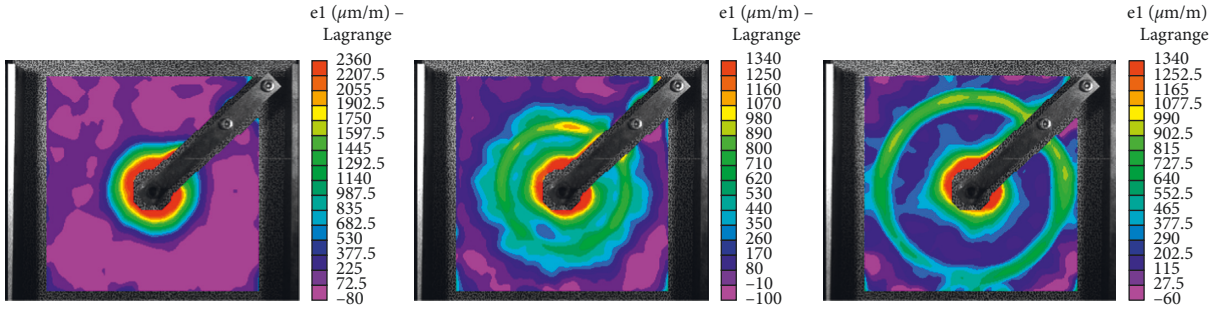

Figure 4: Evolution process of maximum principal strain. (a) $t = 30\,\mu$s, (b) $t = 60\,\mu$s, and (c) $t = 90\,\mu$s.

experiment system can provide sufficient accuracy for full field strain measurement under blasting loading.

The radial strain ε_ρ and the circumferential strain ε_θ within 100 μs after detonation are extracted. During this period, the blasting stress wave propagates in the specimen plane without reaching the boundary of the specimen, so no reflection of the stress wave occurred. The radial strain and circumferential strain of the eight gauging points on each specimen are extracted and subjected to denoising to obtain the strain curves as shown in Figures 6 and 7. In the figures, tensile strain is positive, and compressive strain is negative. Under the action of blasting stress wave, the radial direction of the gauging point is subjected to compressive stress, and the circumferential direction is subjected to tensile stress due to the Poisson effect of material. After blasting stress wave acts on a certain gauging point, the elastic strain accumulated in the medium is released, the radial compressive strain gradually decreases, and the stress state is even changed from compressive to tensile. For specimen T1 and T2, from the gauging points G1 to G8, peaks of the radial strain and circumferential strain gradually decay as the distance from borehole gradually increases.

Under blasting loading, the relationship between stress attenuation and distance satisfies the following equation:

$$\sigma_s = \sigma_0 / \overline{r}^n, \tag{1}$$

where σ_s is the stress peak of a certain gauging point; $\overline{r}$ is the ratio of s (the distance to borehole center) and r (the charge radius); σ_0 is the initial stress at the borehole; and n is the stress attenuation coefficient.

According to the correspondence between stress and strain on the medium, the circumferential stress peak σ_θ and the radial stress peak σ_ρ of the specimens shown in Table 3 are obtained. According to the data in Table 2, the scatter plot of corresponding stress peak in Figure 8 is obtained. It can be found that the stress peak of specimen T1 and T2 is basically equal. It proves that the high stress condition has no obvious effect on the stress peak or the stress change under blasting loading. The circumferential stress peak σ_θ and the radial stress peak σ_ρ are fitted, the attenuation law of σ_θ satisfies that $\sigma_\theta = 884/\overline{r}^{1.80}$, and the attenuation law of σ_ρ satisfies that $\sigma_\rho = -225/\overline{r}^{1.04}$. The attenuation coefficient of the circumferential stress is 1.80, and the attenuation coefficient of the radial stress is 1.04. It can be deduced that

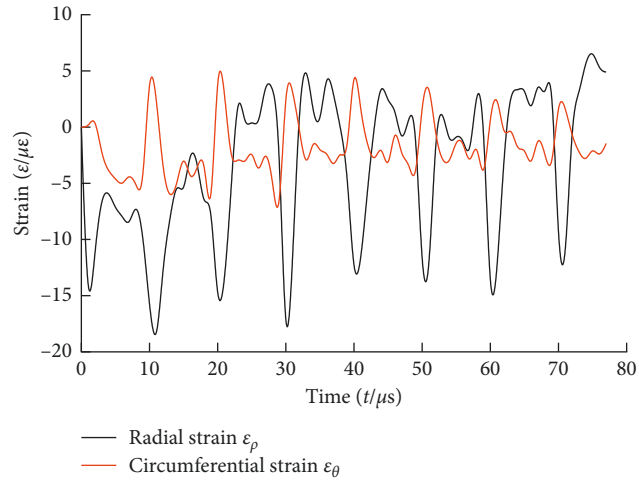

Figure 5: Curves of strain error with time.

circumferential stress peak and the radial stress peak at borehole are, respectively, 884 MPa and −225 MPa.

3.2. Strain Partition. The specimen strain is generated under the action of blasting stress wave. After the action of blasting stress wave, strain at the gauging point is not completely restored, and the unrestored strain is plastic strain. In later stage of the strain curves, the strain hardly changes with time as shown in Figures 6 and 7. Table 4 shows the plastic strain values of gauging points in specimen T1 and T2 under the action of blasting loading, and Figure 9 shows the image relationships corresponding to the relevant data in Table 4. In Table 4 and Figure 9, ε_ρ^p and ε_θ^p, respectively, represent the radial and circumferential plastic strain of gauging points. With increase of the distance s from the borehole, the plastic strain gradually decreases. At G6 (s =12 d) and the following gauging points, the plastic strain is basically stable at a small value where the radial plastic strain is less than 100 $\mu\varepsilon$ and the circumferential plastic strain is less than 200 $\mu\varepsilon$. It can be seen that G6 is a turning point of plastic deformation of the specimen under the action of blasting stress wave. When s < 12 d, the plastic strain is larger, and it decreases significantly with the increase of the distance s; when s > 12 d, the plastic strain is smaller and does not change obviously with the increase of the distance s.

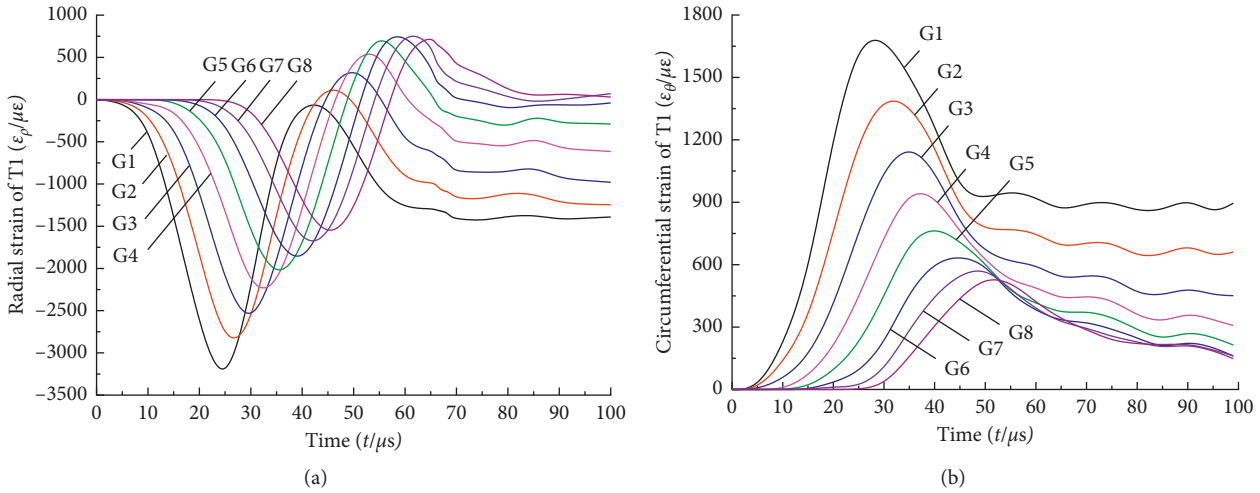

Figure 6: Curves of strain with time in specimen T1. (a) Radial strain and (b) circumferential strain.

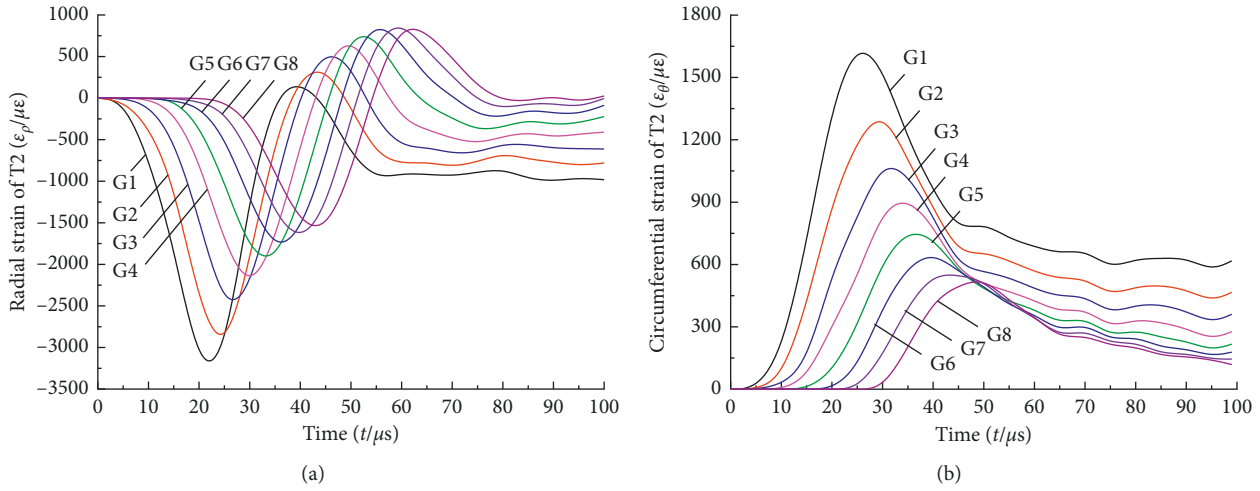

Figure 7: Curves of strain with time in specimen T2. (a) Radial strain and (b) circumferential strain.

Table 3: Stress peaks of gauging points in specimen T1 and T2.

Stress peak/MPa		Gauging point							
Specimen		G1 ($\bar{r}$ = 14)	G2 ($\bar{r}$ = 16)	G3 ($\bar{r}$ = 18)	G4 ($\bar{r}$ = 20)	G5 ($\bar{r}$ = 22)	G6 ($\bar{r}$ = 24)	G7 ($\bar{r}$ = 26)	G8 ($\bar{r}$ = 28)
T1	σ_θ	7.60	6.28	5.12	4.16	3.41	2.80	2.59	2.32
	σ_ρ	−14.55	−12.73	−11.37	−10.23	−9.10	−8.50	−7.73	−6.91
T2	σ_θ	7.73	6.03	4.87	3.96	3.30	2.87	2.41	2.25
	σ_ρ	−14.64	−12.96	−11.05	−10.01	−8.64	−8.10	−7.50	−6.82

According to conventional blasting theory, under the action of blasting loading, areas around the borehole [17] are crushing area, fractured area, and elastic vibration area from the near to the distant. That is, the surrounding medium of borehole is crushed dramatically under strong blasting loading to form the crushing area; subsequently, driven by the quasistatic action of the blasting gas, some of the microcracks in the crushing area are extended to longer radial and circumferential cracks to form the fractured area. In the periphery of the fractured area, it is considered that the effect of blasting stress wave and blasting gas is not sufficient to cause further damage to the medium, which is called elastic vibration area. In this experiment, due to the small charge amount, there is no obvious crushing area or

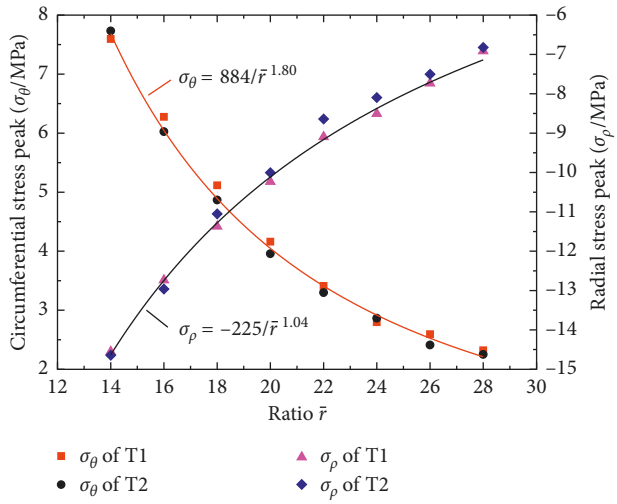

Figure 8: Stress peaks and fitting curves of gauging points.

Table 4: Plastic strains of gauging points in specimen T1 and T2.

Plastic strain/$\mu\varepsilon$		Gauging point							
Specimen		G1 ($\bar{r}$ = 14)	G2 ($\bar{r}$ = 16)	G3 ($\bar{r}$ = 18)	G4 ($\bar{r}$ = 20)	G5 ($\bar{r}$ = 22)	G6 ($\bar{r}$ = 24)	G7 ($\bar{r}$ = 26)	G8 ($\bar{r}$ = 28)
T1	ε_ρ^p	−1442	−1201	−854	−556	−287	48	51	48
	ε_θ^p	883	652	465	355	281	171	170	164
T2	ε_ρ^p	−950	−756	−615	−483	−272	−79	30	28
	ε_θ^p	624	463	340	268	205	152	150	145

fractured area around the borehole. Therefore, the propagation characteristic of blasting stress wave in the abovementioned elastic vibration area is mainly studied. Through above analysis of measured strain, it is found that strain of gauging point in the elastic vibration area is not all "elastic." In the area of $s < 12$ d, the plastic strain is relatively large, and the decay trend is significant with s, and such area can be called "plastic area." In the area of $s > 12$ d, the plastic strain stabilizes in a small range, and such area can be called "quasielastic area.". In view of this, the definition of "elastic vibration area" is not rigorous. Based on the experimental results, it is suggested that the "elastic vibration area" in traditional blasting partition should be further modified as "plastic area" and "quasielastic area."

For both specimen T1 and T2, the boundary of "plastic area" and "quasielastic area" is the position of gauging point G6 ($s = 12$ d), so the high stress condition of specimen T2 has no obvious effect on the division of "plastic area" and "quasielastic area." By comparing the plastic strain and its variation trend in the plastic area shown in Figure 9, it is found that both radial plastic strain and circumferential strain of the gauging points in the plastic area of specimen T2 are smaller than those correspondingly of specimen T1. In addition, in the plastic area, the plastic strain attenuation of gauging points in specimen T2 is relatively slow with the distance s. That is, the plastic strain decay rate of gauging points in specimen T2 is always smaller than that in specimen T1.

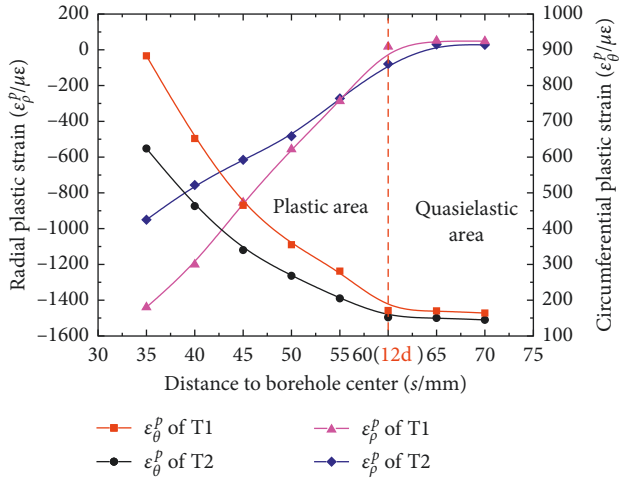

Figure 9: Plastic strains of gauging points.

4. Conclusion

By combined loading of high static stress and dynamic blasting stress, full field strain evolution of blasting under high stress condition is studied. Experimental results show that the high stress condition has no obvious effect on the propagation and attenuation of blasting stress wave. The circumferential stress peak σ_θ and the radial stress peak σ_ρ

are fitted, the attenuation law of σ_θ satisfies that $\sigma_\theta = 884/\overline{r}^{1.80}$, and the attenuation law of σ_ρ satisfies that $\sigma_\rho = -225/\overline{r}^{1.04}$. The attenuation coefficient of the circumferential stress is 1.80, and the attenuation coefficient of the radial stress is 1.04.

Based on the experimental results, the definition of "elastic vibration area" is not rigorous. It is suggested that the "elastic vibration area" in traditional blasting partition should be further modified as "plastic area" ($s < 12$ d) and "quasielastic area" ($s > 12$ d). The high stress condition has no obvious effect on the division of "plastic area" and "quasielastic area." While in the plastic area, both plastic strain and its decay rate of gauging points in high stress condition ($\sigma = 6$ MPa) are smaller than those in normal stress condition ($\sigma = 0$ MPa).

Nomenclature

σ: Static stress applied by jack
d: Borehole diameter
s: Distance between gauging point and borehole
t: Time
ε_ρ: Radial strain
ε_θ: Circumferential strain
σ_s: Stress peak
σ_0: Initial stress at borehole
r: Charge radius ($r = d/2$)
$\overline{r}$: Ratio of s and r
n: Stress attenuation coefficient
σ_θ: Circumferential stress peak
σ_ρ: Radial stress peak
ε_ρ^p: Radial plastic strain
ε_θ^p: Circumferential plastic strain.

Data Availability

The data used to support the findings of this study are available from the corresponding author upon request.

Conflicts of Interest

The authors declare that they have no conflicts of interest.

Acknowledgments

This research was supported by the National Key Research and Development Program of China (no. 2016YFC0600903) and the National Natural Science Foundation of China (no. 51664007).

References

[1] M. C. He, H. P. Xie, and S. P. Peng, "Study on Rock Mechanics in Deep Mining Engineering," *Chinese Journal of Rock Mechanics and Engineering*, vol. 24, no. 16, pp. 2803–2813, 2005.

[2] W. B. Lu, M. Chen, and X. Geng, "A study of excavation sequence and contour blasting method for underground powerhouses of hydropower stations," *Tunnelling and Underground Space Technology*, vol. 29, no. 29, pp. 31–39, 2012.

[3] H. K. Kutter and C. Fairhurst, "On the fracture process in blasting," *International Journal of Rock Mechanics and Mining Sciences*, vol. 8, no. 3, pp. 181–202, 1971.

[4] Y. Bai, W. C. Zhu, and C. H. Wei, "Numerical simulation on two-hole blasting under different in-situ stress conditions," *Rock and Soil Mechanics*, vol. 34, pp. 466–471, 2013.

[5] L. Y. Yang, R. S. Yang, and P. Xu, "Experimental study on the effect of initial compression stress field on blast-induced crack behavior," *Journal of China Coal Society*, vol. 38, no. 3, pp. 404–410, 2013.

[6] P. Yan, T. Li, and W. B. Lu, "Properties of excavation damaged zone under blasting load in deep tunnels," *Rock and Soil Mechanics*, vol. 34, pp. 451–457, 2013.

[7] C. H. Wei, W. C. Zhu, and Y. Bai, "Numerical simulation on the cutting seam cartridge blasting under different in-situ stress conditions," *Explosion and Shock Waves*, vol. 36, no. 2, pp. 161–169, 2016.

[8] H. P. Rossmanith, R. E. Knasmillner, and A. Daehnke, "Wave propagation, damage evolution, and dynamic fracture extension. Part II, blasting," *Materials Science*, vol. 32, no. 4, pp. 403–410, 1996.

[9] W. Z. Cao, X. B. Li, and M. Tao, "Vibrations induced by high initial stress release during underground excavations," *Tunnelling and Underground Space Technology*, vol. 53, pp. 78–95, 2016.

[10] L. X. Xie, W. B. Lu, and Q. B. Zhang, "Analysis of damage mechanisms and optimization of cut blasting design under high in-situ stresses," *Tunnelling and Underground Space Technology*, vol. 66, pp. 19–33, 2017.

[11] T. C. Chu, W. F. Ranson, and M. A. Sutton, "Applications of digital-image-correlation techniques to experimental mechanics," *Experimental Mechanics*, vol. 25, no. 3, pp. 232–244, 1985.

[12] F. X. Chen, X. Chen, and X. Xie, "Full-field 3D measurement using multi-camera digital image correlation system," *Optics and Lasers in Engineering*, vol. 51, no. 9, pp. 1044–1052, 2013.

[13] S. H. Dai, L. M. Dai, and Y. S. Pan, "Concrete stress intensity factor evaluation with a digital image correlation approach," *Journal of Testing and Evaluation*, vol. 44, no. 1, pp. 615–624, 2016.

[14] M. R. Mitchell, R. E. Link, and J. H. Jiang, "Constitutive equations of sheet stamping steel based on DIC measurement," *Journal of Testing and Evaluation*, vol. 39, no. 3, pp. 442–447, 2011.

[15] C. He, J. Yang, and Q. Yu, "Laboratory study on the dynamic response of rock under blast loading with active confining pressure," *International Journal of Rock Mechanics and Mining Sciences*, vol. 102, pp. 101–108, 2018.

[16] Z. Xu, J. Yang, and L. Guo, "Study of the splitting crack propagation morphology using high-speed 3D DIC," *Explosion and Shock Waves*, 2016.

[17] R. S. Yang, C. X. Ding, and Y. B. Wang, "Action-effect study of medium under loading of explosion stress wave and explosion gas," *Chinese Journal of Rock Mechanics and Engineering*, vol. 35, pp. 3501–3506, 2016.

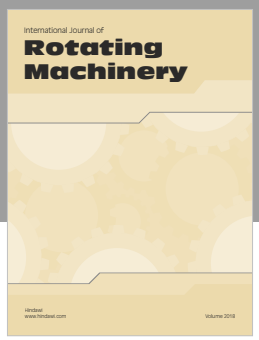

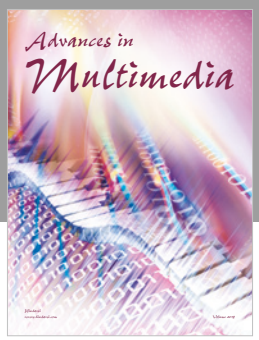

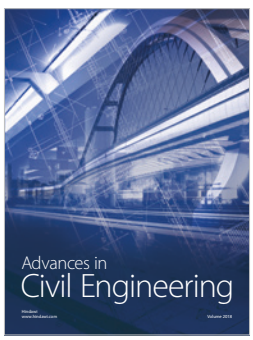

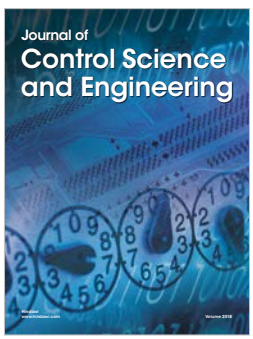

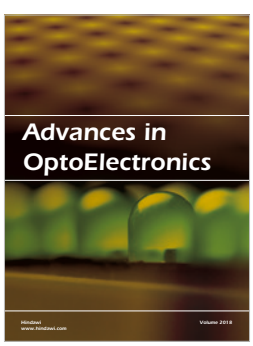

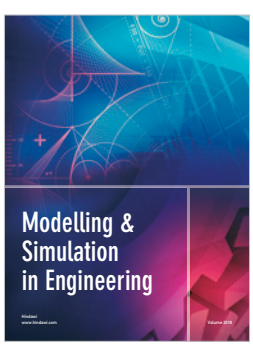

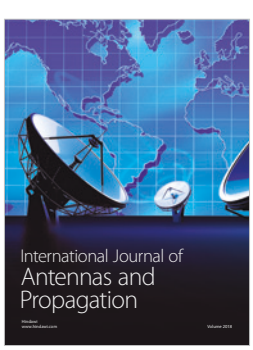

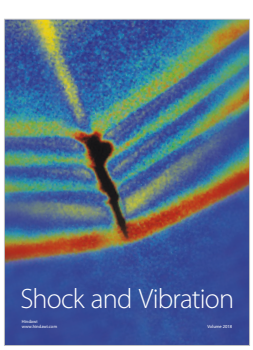

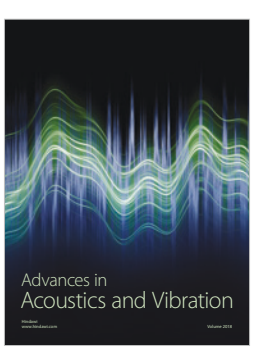

Hindawi

Submit your manuscripts at
www.hindawi.com